Development of a balloon-borne instrument for CO_2 vertical profile observations in the troposphere

Mai Ouchi[1], Yutaka Matsumi[1*], Tomoki Nakayama[2], Kensaku Shimizu[3], Takehiko Sawada[3], Toshinobu Machida[4], Hidekazu Matsueda[5], Yousuke Sawa[5], Isamu Morino[4], Osamu Uchino[4], Tomoaki Tanaka[6,a], Ryoichi Imasu[7]

[1]Institute for Space-Earth Environmental Research and Graduate School of Science, Nagoya University, Furo-cho, Chikusa-ku, Nagoya 464-8601, Japan

[2]Graduate School of Fisheries and Environmental Sciences, Nagasaki University, 1-14, Bunkyo-machi, Nagasaki, Nagasaki 852-8521 Japan

[3]Meisei Electric co., Ltd., 2223 Naganumamachi, Isesaki-shi, Gunma 372-8585, Japan

[4]National Institute for Environmental Studies, 16-2 Onogawa, Tsukuba, Ibaraki 305-8506 Japan

[5]Meteorological Research Institute, Japan Meteorological Agency, 1-1 Nagamine, Tsukuba, Ibaraki 305-0052, Japan

[6]Japan Aerospace Exploration Agency Earth Observation Research Center, 2-1-1, Sengen, Tsukuba, Ibaraki 305-8505, Japan

[7]Atmosphere and Ocean Research Institute, The University of Tokyo, 5-1-5, Kashiwanoha, Kashiwa, Chiba 277-8568, Japan

[a]now at: NASA Ames Research Center, Moffett Field Mountain View CA 94035, USA

Corresponding author: matsumi@nagoya-u.jp

Abstract

A novel, practical observation system for measuring tropospheric carbon dioxide (CO_2) concentrations using a non-dispersive infrared analyzer carried by a small helium-filled balloon (CO_2 sonde), has been developed for the first time. Onboard calibrations, using CO_2 standard gases, is possible to measure the vertical profiles of atmospheric CO_2 with a 240–400 m altitude resolution. The standard deviations (1σ) of the measured mole fractions in the laboratory experiments using a vacuum chamber at a temperature of 298 K were approximately 0.6 ppm at 1010 hPa and 1.2 ppm at 250 hPa. Compared with in situ aircraft data, although the difference up to the altitude of 7 km was 0.6±1.2 ppm, this bias and difference were within the precision of the CO_2 sonde. In field experiments, the CO_2 sonde detected an increase in CO_2 concentration in an urban area and a decrease in a forested area near the surface. The CO_2 sonde was shown to be a useful instrument for observing and monitoring the vertical profiles of CO_2 concentration in the troposphere.

1. Introduction

Atmospheric carbon dioxide (CO_2) is one of the most important anthropogenic greenhouse gases for global warming. Certain human activities, such as fossil fuel combustion, cement production, and deforestation are the major cause of atmospheric CO_2, making the global average concentration of atmospheric CO_2 to increase from 280 ppm before the Industrial Revolution to 400.0 ppm in 2015 (World Meteorological Organization, WMO 2016). Over the last 10 years, the rates of atmospheric CO_2 increase is measured at 2.21 ppm yr^{-1} (WMO 2016). Atmospheric CO_2 is measured by ground-based stations and ships using the flask sampling and continuous instrument methods such as non-dispersive infrared absorption (NDIR) (Tanaka et al. 1983, Hodgkinson et al. 2013) and cavity ring-down spectroscopy (CRDS) (Winderlitch et al. 2010). A network of ground-based Fourier transforms spectrometers (FTS), that record the direct solar spectra in the near-infrared spectral region (Total Carbon Column Observing Network, TCCON), is used to observe the column-averaged mole fraction of CO_2 in dry air (total column XCO_2) (Wunch et al. 2011). These observations have provided an extensive information, regarding the distribution and temporal variation of CO_2 in the atmosphere (Pales and Keeling, 1965; Conway et al. 1988; Komhyr et al. 1989; Tans et al. 1989; Conway et al. 1994). Moreover, atmospheric CO_2 measurements data are useful for estimating CO_2 fluxes at the surface through inverse modeling (Gurney et al. 2004; Baker et al. 2006). Due to the limited number of observation sites and the limitations of their altitudinal range, a large degree of uncertainty in the current estimates of the regional CO_2 sources and sinks is noted (Gurney et al. 2002). More atmospheric CO_2 measurements are needed to reduce the uncertainties in CO_2 fluxes estimation using an inverse modeling.

To address the issues with insufficient CO_2 observational data, satellite remote sensing techniques have been used to investigate the CO_2 distribution on a global scale (Chédin et al. 2002; Crevoisier et al. 2004; Dils et al. 2006). The Greenhouse Gases Observing SATellite (GOSAT), which measures the short wavelength infrared (SWIR) spectra of sunlight reflected by the earth's surface with a Fourier

63 transform spectrometer and obtains the total column XCO_2, has been in operation since early 2009
64 (Yokota et al. 2009; Yoshida et al. 2011; Morino et al. 2011). Since 2014, the Orbiting Carbon
65 Observatory-2 (OCO-2) satellite has also measured the IR spectra of the surface reflected sunlight
66 with a diffraction grating spectrometer and obtains total column XCO_2 (Eldering et al. 2017). However,
67 these satellite observations provide only nadir total column XCO_2, and do not measure the vertical
68 distributions of CO_2 concentrations, as the observed spectra of the surface-reflected sunlight do not
69 provide enough information to determine the vertical distributions. Furthermore, the satellites overpass
70 a specific earth-based target once several days only at about noon in the solar time because of their
71 sun-synchronous orbits.

72 The altitude distributions of CO_2 concentrations has been measured using other techniques. For
73 instance, tall towers measure vertical profiles of CO_2 near the ground (Bakwin et al. 1992, Inoue and
74 Matsueda, 2001; Andrews et al. 2014). CO_2 vertical profiles up to 10 km near the airports have been
75 observed by the equipment installed by the commercial airlines, such as the Comprehensive
76 Observation Network for TRace gases by Airliner (CONTRAIL program) (Machida et al. 2008;
77 Matsueda et al. 2008). Measurements by equipment installed on chartered aircrafts have also been
78 undertaken, which include the High-performance Instrumented Airborne Platform for Environmental
79 Research (HIAPER), Pole-to-Pole Observations (HIPPO) program up to 14 km in the altitude spanning
80 the Pacific from 85° N to 67° S (Wofsy et al. 2011), the NIES/JAXA (National Institute of
81 Environmental Studies and Japan Aerospace eXploration Agency) program at an altitude from 2 to 7
82 km (Tanaka et al. 2012), and the NOAA/ESRL Global Greenhouse Gas Reference Network Aircraft
83 Program (Sweeney et al. 2015). Although these aircraft measurements provided the vertical profiles
84 of CO_2 concentrations, they had the short-term observation campaigns in the limited areas or
85 measurements around a limited number of large airports used by the commercial airlines. The
86 continuation and expansion of airborne measurement programs for CO_2 and related tracers are
87 expected to enhance the estimation of the global carbon cycling greatly (Stephens et al., 2007).

Atmospheric CO_2 observations using balloons, to select specific locations unless prohibited or restricted by aircraft flight paths, are useful for solving the issues associated with the sparseness of CO_2 vertical data. Balloon-borne observations of stratospheric CO_2 are previously conducted by other studies. For instance, stratospheric air sampling was conducted using a cryogenic sampler onboard balloons once a year from 1985 to 1995 over the northern part of Japan (Nakazawa et al. 1995). Balloon-borne near-infrared tunable diode laser spectrometers have been developed to provide in situ data for CO_2 in the stratospheric atmosphere (Durry et al. 2004; Joly et al. 2007, Ghysels et al. 2012). Furthermore, two in situ CO_2 analyzers adopting the NDIR technique, using a modified commercial detector for stratospheric measurements, have been developed for deployment on the NASA ER-2 aircraft and on a balloon (Daube et al. 2002). These balloon borne instruments described above were specially designed to measure CO_2 concentrations in the stratosphere.

Observation of the CO_2 vertical distribution in the troposphere is essential because the uncertainties in the estimated fluxes, using the inverse method, can be attributed to the inaccurate representations of the atmospheric processes in transport models. Misrepresentation of vertical mixing by the transport models, particularly inside of the boundary layer, which is the layer closest to the ground where CO_2 is taken up and released, is one of the dominant causes of the uncertainty in CO_2 flux estimation (Stephens et al. 2007; Ahmadov et al. 2009). Recently, the observation of tropospheric CO_2 was conducted, using a lightweight unmanned aerial vehicle, such as a kite plane, with a commercial NDIR instrument. CO_2 profiles were observed in and above the planetary boundary layer up to 2 km to investigate the temporal and spatial variations of CO_2 (Watai et al. 2006). A passive air sampling system for atmospheric CO_2 measurements, using a 150 m long stainless-steel tube called an AirCore was developed (Karion et al. 2010). The AirCore mounted on an airplane or a balloon ascends with evacuating inside of the tube to a high altitude of 30 km at flight maximum, then, collecting ambient air by pressure changes along a decrease in altitude. The sampled air in the tube is analyzed with the precision of 0.07 ppm for CO_2 indicated as one standard deviation in the laboratory and the vertical

profile of CO_2 is obtained.

In the present study, we have developed a practical CO_2 sonde system that can measure in situ CO_2 vertical profiles in the atmosphere from the ground to altitudes up to about 10 km with a 240–400 m altitude resolution by using a small-sized balloon. Although the sonde system is thrown away after every flight due to the difficulties associated with recovery, the sonde systems are easily prepared with a relatively low cost. We have tested the sonde flight experiments more than 20 times in Japan. The CO_2 sonde developed has the following advantages, compared with other measurement techniques described above: (1) its cost of operation is low and the flight permission is easy to obtain from the authorities as compared with the aircraft observations; (2) the CO_2 sonde can be easily carried to the launch sites since the instrument is light; (3) a limited amount of power is required for the operation; (4) it can generally be launched at any time; and (5) the meteorological data are obtained simultaneously with CO_2 profile data. In this study, the design of our novel CO_2 sonde and the results of the comparison experiments with aircraft measurements are described. The target accuracy and precision in the measurements with the CO_2 sonde are below about 1 ppm CO_2 mole fraction in the atmosphere of 400 ppm CO_2, preferable for carbon cycle studies (e.g. Maksyutov et al. 2008). The developed CO_2 sonde system attained virtually all the targets from the ground to an altitude of about 10 km.

Inai et al. (2018) measured vertical profiles of CO_2 mole fraction in the equatorial eastern and western Pacific in February 2012 and February–March 2015, respectively, by using our novel CO_2 sondes which are described in this report. They found that the 1–10 km vertically averaged CO_2 mole fractions lie between the background surface values in the Northern Hemisphere (NH) and those in the Southern Hemisphere (SH) monitored at ground-based sites during these periods. Their study showed that the combination of CO_2 sonde measurements and trajectory analysis, taking account of convective mixing, was a useful tool in investigating CO_2 transport processes.

2. Materials and methods

a. Design of the CO_2 sonde

Many severe restrictions are noted for the operation of balloon-borne CO_2 sondes. First, the weight of the CO_2 sonde package should be less than about 2 kg, based on the legal restriction by the US FAA (Federal Aviation Administration) and by the Japanese aviation laws for the payload weight of 2.721 kg for unmanned free balloons. Balloon systems heavier than the above regulation weight are not useful for the frequent flights because the flight permission from the authorities is much more difficult to obtain, and the additional safety requirements are more expensive. The balloon system is thrown away in the ocean after each flight due to a long-distance transportation (100 km or more to the east) by strong westerly winds in the upper atmosphere of mid-latitude area. This is done to avoid the accidents associated with a falling onto the urban areas, resulting in high recovery costs. Therefore, the cost of the CO_2 sonde system should be low for frequent observations. The non-recovery system implies that every instrument should perform consistently.

In this study the NDIR technique was adopted for a detection of CO_2 concentrations. The NDIR CO_2 measurement techniques have been widely used in many places such as WMO/GAW (Global Atmosphere Watch) stations. Our target instrumental accuracy and precision of approximately 1 ppm are less stringent than those of the ground-based instruments (± 0.1 ppm) used at the WMO/GAW stations (WMO, 2016). However, the surrounding conditions for the instrument are substantially severe during the flight experiments, as the pressure changes from 1,000 to 250 hPa and the surrounding temperature changes from 300 to 220 K during flights from the surface to an altitude of 10 km in about 60 min.

In the NDIR technique for CO_2 measurements, the IR emission from a broadband wavelength source is passed through an optical cell and two filters, and then the light intensities are detected by two IR detectors. The one optical filter covers the whole absorption band of CO_2 around 4.3 μm, while the other covers a neighboring non-absorbed region around 4.0 μm. provided that the chosen active and

reference channel filters do not significantly overlap with the absorption bands of other gas species present in the application. (Hodgkinson et al., 2013).

The Beer–Lambert Law is expressed by Eq. (1), defining the light intensity in the absence of CO_2 in the cell as I_0 and the light intensity in the presence of CO_2 in the cell as I,

$$\frac{I}{I_0} = \exp(-\varepsilon C L) \qquad (1),$$

where C is the CO_2 concentration in molecules cm^{-3}, L is the optical path length in cm, and ε is the absorption cross-section in cm^2 $molecule^{-1}$. Using the relationship of $C = XP(k_B T)^{-1}$, where X is the CO_2 mole fraction and P is the pressure of dehumidified ambient air, and the approximation of $\exp(-\varepsilon C L) = 1 - \varepsilon C L$, under the condition of $\varepsilon C L << 1$, Eq. (1) is rewritten as:

$$\frac{(I_0 - I)}{P} = X \frac{I_0 \varepsilon L}{k_B T_C} \qquad (2),$$

where T_c is the sample air temperature in the sensor cell and k_B is the Boltzmann constant. With a 120 mm long absorption cell, the absorption intensity is approximately 3% at 400 ppm CO_2 with our CO_2 NDIR system, i.e., $\varepsilon CL \approx 0.03$ and the approximation of $\exp(-\varepsilon C L) = 1 - \varepsilon C L$ are well fitted. The values of $[I(4.0) - I(4.3)]$ were used instead of $(I_0 - I)$ to obtain the CO_2 mole fraction values in the NDIR measurements, where $I(4.0)$ and $I(4.3)$ were the signal intensities at the 4.0 μm wavelength for background measurements and the 4.3 μm wavelength for CO_2 absorption measurements, respectively. Thus, the value of $[I(4.0) - I(4.3)]/P$ is thus proportional to the CO_2 mole fraction X in the optical cell. The proportional constant is usually determined by the measurements of the standard gases. In the NDIR measurements at the ground WMO/GAW stations, carbon dioxide mole fractions are referenced to a high working standard and a low working standard and are determined by the interpolations of the signals with the two standards, and the calibration with the two standard gases are carried out every 12 h (Fang et al., 2014).

b. System configuration of the CO_2 sonde system

A schematic diagram and photograph of the CO_2 measurement instrument are shown in Fig. **1**. The CO_2 sonde has three inlets installed for ambient air and two calibration gases with mesh filters (EMD Millipore, Millex-HA, 0.45 μm pore size) to remove the atmospheric particles. Three solenoid valves (Koganei, G010LE1-21) were used to switch the gas flow to the CO_2 sensor. A constant-volume piston pump with a flow rate of 300 cm^3 min^{-1} (Meisei Electric co., Ltd.), which is originally used for ozonesonde instruments, directed the gas flows from the inlets through the solenoid valves into a dehumidifier, a flow meter, and a CO_2 sensor. The absolute STP (standard temperature and pressure) flowrate decreased with a decrease in pressure. Since the exit port of the CO_2 sensor was opened to the ambient air, the pressure of dehumidified outside air and calibration gases in the absorption cell were equal to the ambient pressure during the flight. Next to the pump, the gases were introduced to a glass tube filled with the magnesium perchlorate grains (dehumidifier) installed upstream to the CO_2 sensor to remove the water vapor. Fabric filters were installed on both ends of the dehumidifier, and a mesh filter was installed downstream of the dehumidifier to prevent the CO_2 sensor from the incursion of magnesium perchlorate grains to the optical cell. The flow from the piston pump had pulsation and the dehumidifier vessel worked as a buffer to reduce the pulsation.

The infrared absorption cell consisted of a gold-coated glass tube, a light source, and a photodetector. The light source (Helioworks, EP3963) consisted of a tungsten filament with a spectral peak intensity wavelength of approximately 4 μm. The light from the source passed through a gold-coated glass tube (length 120 mm, and inside diameter 9.0 mm). The commercial CO_2 NDIR photodetector (Perkin-Elmer TPS2734) had two thermopile elements, one of which was equipped with a band-pass filter at a wavelength of 4.3 μm for the measurement of the CO_2 absorption signal, whereas the other was equipped with a band-pass filter at a wavelength of 4.0 μm for the measurement of the background signal. The signals from the sensors were amplified by an operational amplifier and converted to 16 bit digital values by an A/D convertor. The signal intensities of the detectors at 4.0 and 4.3 μm without CO_2 gas were set to the equal levels by adjusting the amplification factors in the laboratory. The electric

power for the CO_2 sensor, pump, and valves was supplied through a control board using three 9 V lithium batteries, lasted for more than 3 h during the flight. The control board connected to the components regulated the measurement procedures, such as switching the solenoid valves and processing the signal. As shown in Fig. **1**, the measurement system has an expanded polystyrene box molded specially to settle the optical absorption cell, electronic board, pump, battery and other components.

We are trying to use more environmentally friendly materials instead of the chemical dehumidifier and polystyrene packing etc.

c. Calibration gas package

Under the wide ranges of temperature and pressure conditions, the CO_2 sensor signal was unstable, and the calibration of the CO_2 sensor only on the ground before launch was insufficient to obtain the precise values of the CO_2 concentrations. To solve this problem, an in-flight calibration system was incorporated into the CO_2 sonde. A calibration gas package was attached to the CO_2 sonde for the in-flight calibration, as shown in Fig. **2**. The calibration gas package consisted of two aluminum coated with polytetrafluoroethylene (PTFE) bags (maximum volume: 20 L), containing reference gases with low (~370 ppm) and high (~400 ppm) CO_2 concentrations. In each bag, ~8 L (STP) of the reference gas was introduced from standard CO_2 gas cylinders just before launch. Since the gas bags were soft, their inner pressures were equal with the ambient air pressures during the balloon flight. The gas volumes in the bags increased with the altitude during the ascent of the balloon due to a decrease in the ambient pressure, while the reference gases were consumed during the calibration procedures. The optimum amounts of gas in the bags were determined by both the ascending speed of the balloon and the consumption rate to avoid the bursting of the bags and exhaustion of the gases. The CO_2 concentrations of the reference gases in the bags were checked by the NDIR instrument (LICOR, LI-840) before launching. Thereafter, approximately 6 L of the reference gas was left in each bag for a subsequent in-flight calibration. The change in the CO_2 mole fraction in the bags was less than 1 ppm

over a 3 days period, which was negligible over the observations time during the balloon flight. All measurements were reported as dry-air mole fractions relative to the internally consistent standard scales maintained at Tohoku University (Tanaka et al. 1987; Nakazawa et al. 1992).

Since the gas exit port of the optical absorption cell was opened to the ambient air, the cell pressure was equalized with the ambient pressure for measuring both the ambient air and two standard gases. During the balloon-borne flights, the temperatures inside the CO_2 sonde package were measured with thermistors. The temperature inside the CO_2 sonde package gradually decreased by approximately 5 K, from 298 K on the ground to 293 K at an altitude of 10 km during the flights. Probably due to the polystyrene box, and the heat produced by the NDIR lamp, pump and solenoid valves, temperature inside the sonde package remained virtually constant in spite of low ambient temperatures at high altitudes (~220 K). Within one measurement cycle time (160 s) with the standard gases, the temperature change was less than 0.4 K in the sonde package. The temperatures of the sample gas in the tube just before the inlet of the CO_2 NDIR cell were also measured using a thin wire thermistor, commonly used for ambient temperature measurement in GPS sonde equipment with a quick response time (shorter than 2 s). The gas temperature change was negligible at the valve change timings between the standard gas and ambient air (< 0.1 K). The result indicated that the gas temperatures were relatively constant after passing through the valves, pump, dehumidifier cell, and piping for both the standard gases and ambient air.

The performances of the CO_2 sonde instruments were checked before the balloon launching since the CO_2 sonde systems were not recovered after the launch experiments were performed. For about 60 min. before the launch, the values of $\left[I(4.0) - I(4.3)\right]/P$ were measured with the valve cycles (each step 40 s, total 160 s) for two standard gas packages (~370 ppm and ~400 ppm) for calibration and one intermediate concentration gas package (~385 ppm) as a simulated ambient gas sample.

d. Total sonde system

The CO_2 sonde was equipped with a GPS radiosonde (Meisei Electric co., Ltd., RS-06G). The balloon carried the instrument packages in the altitude with measuring CO_2 and meteorological data (GPS position and time, temperature, pressure, and humidity). The CO_2 sonde transmitted those data to a ground receiver (Meisei Electric co., Ltd., RD-08AC) at 1 s intervals, thus it was unnecessary to recover the CO_2 sonde after the balloon burst. Figure **2** showed an overall view of the CO_2 sonde developed in this study, which consisted of a CO_2 measurement package, a calibration gas package, a GPS radiosonde, a balloon, and a parachute. The total weight of the CO_2 sonde was 1700 g, including the GPS radiosonde (150 g), CO_2 measurement package (1000 g), and calibration gas package (550 g). The dimensions of the CO_2 measurement package were width (W) 280 mm × height (H) 150 mm × depth (D) 280 mm. The size of the calibration gas package was W 400 mm × H 420 mm × D 490 mm.

The CO_2 sonde system was flown by a 1200 g rubber balloon (Totex). The ascending speed was around 4 m / s by controlling the helium gas amount in the rubber balloon and checking the buoyancy force. In practice, it was difficult to precisely control the ascending speed of the balloon, and the actual resulting speeds were in the range of 3 - 5 m s^{-1}. This corresponds to the height resolution of approximately 240–400 m for the measurements of the CO_2 vertical profiles.

Ascending speed slower than 3 m s^{-1} can lead to a collision with a nearby tree and building, result in equipment falling in the urban areas. With faster ascending speeds, the altitude resolution of the measurements decreased and the gas standard bag became full and the pressure inside the gas bags became higher than the ambient pressure because of the lower ambient pressures at higher altitudes. The high pressure inside the gas bag resulted in the fast flow speed in the optical absorption cell of NDIR, which shifted the signal values for the pressurized gas sample. Since pressure relief valves for the bags did not work at low pressures at high altitudes, we did not use the pressure relief valve for the standard gas bags. When the ascending speed was low, the standard gas bags became empty since they were consumed by the in-flight calibration procedures during the long ascending time. Since the measurements after the over-pressurization or the exhaustion of the reference gas bag are useless, this

technical problem determines the upper limit (10 km) of altitude for the measurements in this study. Based on our experiences, this problem generally occurred at an altitude above approximately 10 km.

e. Data processing procedures

Since the surrounding conditions of the sonde change significantly during the ascending period, the NDIR measurement system is calibrated with the two standard gases at every altitudes. However, since the balloon-borne instrument is only equipped with one NDIR absorption cell and the balloon ascends continuously, it is not possible to measure the ambient air sample and the two standard gases at the same time and at the same altitude. Therefore, the measurement cycle during the flights consisted of the following steps: (1) low concentration standard gas, (2) ambient air, (3) high concentration standard gas, and (4) ambient air. The measurement time for each step was 40 s. At switching timings of the valve cycles, the signal became stable within 10 s, and the averages of residual 30-s period signals were used for the calculation of the CO_2 mole fractions. Since the gas exit port of the NDIR optical absorption cell was opened to the ambient air, the cell pressure was equalized with the ambient pressure. During the period of the 40 s gas change, the pressure would change about 2 % when the ascending speed of the balloon was 4 m s^{-1}. The temperature of the ambient air and standard gas samples at the inlet port of the optical cells was measured and found to be constant during each cycle of the calibration procedure.

Figure **3** shows an example of the raw data obtained from the CO_2 sonde experiment. Figure 3 presents the plots of the values of $[I(4.0)-I(4.3)]/P$ against the altitude, where $I(4.0)$ and $I(4.3)$ are the signal intensities at the wavelength of 4.0 μm for background measurements and the 4.3 μm wavelength for CO_2 absorption measurements, as obtained by the NDIR CO_2 sensor on the balloon, and P is the ambient atmospheric pressure obtained by the GPS sonde data and pressure measurements on the ground.

The values of $[I(4.0)-I(4.3)]/P$ are proportional to the CO_2 mole fraction X according to the

Beer-Lambert law as expressed by Eq. (2). By using the values of $[I(4.0)-I(4.3)]/P$, we can compensate for the pressure change to determine the CO_2 concentration. As shown in Fig. **3**, the differences in the $[I(4.0)-I(4.3)]/P$ values between the low and high standard gases remained relatively constant while ascending to the higher altitudes. However, the $[I(4.0)-I(4.3)]/P$ values for the each standard gas did not change linearly but sometimes displayed some curvatures as shown in Fig. **3**. This may be due to the differences between the baseline drift of the two sensors at 4.3 μm and 4.0 μm in the NDIR detector. Since the measurements were performed alternately for the standard gases and the ambient air with the NDIR cell and are not performed simultaneously, the values for the standard gas signals at the time of the ambient air measurement was estimated. Therefore, the cubic spline fitting curves for the observation points of the 30 s average values (red circles in Fig. **3**) of the same standard gas were used to obtain the low and high calibration points for the calculation of the mole fractions in the ambient air. In Fig. **3**, the cubic spline fitting curves are represented by the red curves, and the estimated values for the standard gases at the ambient gas measuring time are represented by the small black dots on the cubic spline curves, which are used for the interpolation to determine the ambient air concentrations. Linear line fitting between the standard gas values did not work well because the connection lines of the values sometimes displayed curvatures as shown in Fig. **3**. Since there were in-phase fluctuations in the $I(4.0)$ and $I(4.3)$ signals during the flights, the subtraction of $[I(4.0)-I(4.3)]$ could partly improve the signal-to-noise ratios by canceling in-phase fluctuations with each other.

3. Results and discussion

a. Laboratory tests

Since the linear interpolation method for the $[I(4.0)-I(4.3)]/P$ values was used to determine the ambient air CO_2 mole fractions in the balloon-borne experiments, the deviations from the linear interpolation process were also investigated. The measurements of various mole fractions gas samples

in the laboratory indicated that the linear interpolation error with the two standard gas packages (~370 ppm and ~400 ppm) was less than 0.2 ppm in the range between 360 and 410 ppm. Figure **4** shows the measurement results of the NDIR cell developed in this study at various CO_2 mole fractions. The outlet port of the NDIR system was connected to the commercial CO_2 instrument (LICOR, LI-840A) as a standard device, and the two instrument simultaneously measure the sample gas at 1010 hPa. The standard gases of 365 and 402 ppm were used for the calibration, and the mixtures of the standard gases were used for the samples. This indicated the values of $[I(4.0) - I(4.3)]/P$ of the system were proportional to the mole fraction of CO_2. This type of experiment could not be performed at low pressures, since we did not have a standard device which can be operated under low pressures.

Figure **5** shows the results of an experiment using a vacuum chamber in the laboratory, where the flight pressure conditions were simulated and the performances of the CO_2 sonde instruments was evaluated. The temperature inside the chamber was not controlled and was about 298 K. In the actual flights, the temperature inside the sonde package did not change more than 5 K. The CO_2 sonde system and two standard gas packages were placed in the vacuum chamber. The chamber was filled with the mole fraction sample gas of 377.3 ppm before the pumping. The pressure of the chamber was gradually and continuously decreased using a mechanical pump from 1010 hPa (ground surface pressure) to 250 hPa (about 10 km altitude pressure) over 60 min, corresponded to a balloon ascending speed of 3 m /s in actual flights, whereas the sample gas was slowly and continuously supplied to the chamber. The values $[I(4.0) - I(4.3)]/P$ were measured for the two standard gas packages, and the sample gas with the valve cycles (each step 40 s, total 160 s) as described in the previous section. The mole fractions of the sample gas in the chamber were calculated by the interpolation of the signals for the two standard gases. The 30 s signals 10 s after the valve changes were used for the interpolation calculations to avoid the incomplete gas exchanges in the NDIR optical cell. The black circle in Fig. **5** indicates the sample gas mole fraction obtained from the linearly interpolated standard gas signals in each calibration cycle. The vertical error bar in Fig. **5** indicates the square-root of the sum of squares for the

362 standard deviations of the sample and standard gas signals at each step. The errors in the CO_2 mole
363 fractions were estimated to be 0.6 ppm at 1010 hPa and 1.2 ppm at 250 hPa using the calibration cycles.
364 The results in Fig. 5 indicated that the determination of the sample gas concentration using the linear
365 interpolation with the standard gases was appropriate within the error, when the pressure continuously
366 decreased form 1000 to 250 ppm over 60 min.

367 When the CO_2 sonde instrument was inclined and vibrated in the laboratory, the fluctuations in the
368 signals were observed. The quantitative correlation between the signal fluctuation intensities and
369 acceleration speed, measured by a 3-dimensional acceleration sensor, was investigated, but no distinct
370 correlation was detected. However, the in-flight calibration system partly solved this problem by taking
371 the signal difference of $[I(4.0)-I(4.3)]$ and also by measuring alternately the two standard gases
372 every 40 s during the balloon flights.

373 The temperature characteristics of the CO_2 sensor were also investigated by changing the sensor cell
374 block temperature from 273 to 323 K at the pressure of ~1010 hPa, using a heater in the laboratory.
375 The laboratory experiment related to the temperature dependence suggested that the measurement error
376 is less than 0.2 ppm due to the temperature change during one valve cycle (160 s) in the balloon-borne
377 experiments.

378 In principle, the absorption intensities $(I_0 - I)$ in the NDIR measurements are proportional to the
379 absolute CO_2 concentrations in the sample air in the absorption cell. Therefore, at higher altitudes
380 where the pressures were lower, the values of $[I(4.0)-I(4.3)]$ were smaller and the signal-to-noise
381 ratios of $[I(4.0)-I(4.3)]/P$ decreased. The error of the CO_2 mole fractions of 1.2 ppm at 250 hPa
382 corresponds to an absolute CO_2 concentration of 3.2×10^{13} molecule cm^{-3}. The equivalent altitude for
383 this value was 90 km with a CO_2 molar fraction of 400 ppm. As described previously, the purpose of
384 CO_2 balloon observations is to measure the CO_2 mole fraction within a 1 ppm errors in the atmospheres
385 around 400 ppm CO_2. The upper limit of the altitude for the observations with the developed CO_2
386 sonde is considered to be ~10 km. Furthermore, as described in section 2d, the problems of the vacancy

or over-pressure in the standard gas bags took place around 10 km altitudes, which resulted in large errors. This also practically determines the upper altitude limit for CO_2 sonde observations.

b. Comparison with aircraft data

Two types of aircraft measurement data, the NIES/JAXA chartered aircraft and the CONTRAIL data, were used for comparison with the CO_2 sonde measurement data. The NIES/JAXA chartered aircraft measurements were conducted on the same days as the CO_2 sonde observations (January 31st, 2011 and February 3rd, 2011). The chartered aircraft observations were performed as a part of the campaign for validating the GOSAT data and calibrating the TCCON FTS data at Tsukuba (36.05°N, 140.12°E) (Tanaka et al., 2012). The chartered aircraft data were obtained using an NDIR instrument (LICOR LI-840) that had a control system of constant pressure and had the uncertainty of 0.2 ppm. On both January 31st and February 3rd, the chartered aircraft measured the CO_2 mole fractions during descent spirals over Tsukuba and Kumagaya (Fig. **6**). Because the air traffic was strictly regulated near the Haneda and Narita international airports, the aircraft observations at altitudes above 2 km over Tsukuba were prohibited. Therefore, the descent spiral observations were conducted over Kumagaya at altitudes of 7–2 km and over Tsukuba at altitudes of 2–0.5 km. Tsukuba is located approximately 20 km northeast of Moriya, whereas Kumagaya is located approximately 70 km northwest of Moriya.

Seven profiles based on the CONTRAIL measurements, obtained during the ascent and descent of aircrafts over Narita airport and had passage times close to the CO_2 sonde observations, were available within two days after or before the dates of the CO_2 sonde measurements (Table 1). The CO_2 sonde observations were conducted on January 31st and February 3rd, 2011 from Moriya. One set of CONTRAIL data, obtained from the flight from Hong Kong to Narita (data set name: 11_060d), was available on January 31st, but no CONTRAIL data were available for February 3rd. Therefore, the CONTRAIL data, obtained from the flight from Hong Kong to Narita on February 2nd (data set name: 11_062d), were used for comparison with the February 3rd CO_2 sonde data. Figure **6** also shows the

412 CONTRAIL 11_060d and 11_062d flight paths and the CO_2 sonde launched at Moriya on January 31st
413 and February 3rd, 2011. On January 31st, the flight time of the CONTRAIL 11_060d over the Narita
414 airport and the launch time of the CO_2 sonde at Moriya were relatively close to one another. The flight
415 path of the CONTRAIL 11_062d data on February 2nd, 2011 was close to that of the CO_2 sonde on
416 February 3rd, 2011 and both observations were conducted in the early afternoon. The CONTRAIL
417 data referred in the present study was obtained using the Continuous CO_2 Measuring Equipment
418 (CME) located onboard commercial airliners (Machida et al. 2008; Matsueda et al. 2008). The typical
419 measurement uncertainty (1σ) of the CME has been reported as 0.2 ppm (Machida et al. 2008).
420 Figure **7** shows the vertical profiles of CO_2 observed by the CO_2 sonde at Moriya, the chartered
421 aircraft at Kumagaya and Tsukuba, and the CONTRAIL over the Narita airport on January 31st, 2011.
422 The overall vertical distribution of the CO_2 sonde data resembled with those of the chartered aircraft.
423 The vertical profiles of the CONTRAIL 11_060d flight on January 31st at the 5.3–6.8 km altitude
424 range consisted of the missing data because of the CME calibration period.
425 Figure **8** shows the comparison of the CO_2 vertical profiles obtained by the CO_2 sonde over Moriya,
426 NIES/JAXA chartered aircraft over Kumagaya and Tsukuba on February 3rd, 2011, and the
427 CONTRAIL on February 2nd, 2011 over Narita. The shape of the vertical profile obtained by the
428 chartered aircraft on February 3rd resembled that obtained by the CO_2 sonde, although the profile from
429 the chartered aircraft was shifted to the lower CO_2 concentration side compared to that of the CO_2
430 sonde.
431 Table 2 lists the comparisons of the CO_2 concentrations measured by the balloon CO_2 sonde and
432 NIES/JAXA chartered aircraft on January 31st and February 3rd, 2011. The averaged values of the
433 aircraft measurement over the range of each balloon altitude ± 100 m are listed in Table 2, since the
434 altitude resolution of the aircraft measurements is higher than that of the CO_2 sonde. From the February
435 3rd measurements, the height of the boundary layer around an altitude of 1 km was different between
436 the CO_2 sonde and the NIES/JAXA aircraft measurements as shown in Fig. **8**. Therefore, the data

below 1 km on February 3rd are not included in Table 2. From the data on January 31st, the averaged value of the differences between the CO_2 sonde and the NIES/JAXA aircraft was relatively small (0.42 ppm), which corresponded to the bias of the measurements. The standard deviation of the differences was 1.24 ppm. From the February 3rd data, the bias was large (1.41 ppm), whereas the standard deviation of the differences was not so large (1.00 ppm), which corresponded to the similar but shifted vertical profiles in shapes between the CO_2 sonde and aircraft measurements as shown in Fig. **8**. The difference between the CO_2 sonde data and the NIES/JAXA chartered aircraft data on February 3rd is nearly equal to the difference between CONTRAIL data on February 2nd and the NIES/JAXA chartered aircraft data on February 3rd. The results with both cubic spline and linear interpolation methods were also listed in Table 2 for the balloon-borne experiments on January 31, 2011 in the comparisons with the JAXA-NIES aircraft measurements. This clearly indicates that the cubic spline interpolation method is better than the linear one.

Table 3 lists the comparisons of the CO_2 concentrations measured by the balloon CO_2 sonde and CONTRAIL aircraft, 11_060d on January 31st and 11_062d on February 2nd, 2011 up to the altitude of 7,000 m. The averaged values of the aircraft measurements over the range of each balloon altitude $\pm$ 200 m are listed in Table 3. The biases between the CO_2 sonde and the CONTRAIL aircraft results were relatively small, 0.33 and 0.35 ppm, and the standard deviations of the differences were 1.16 and 1.30 ppm for the results on January 31st and February 3rd, respectively.

From the comparison between the CO_2 sonde data and the aircrafts (NIES/JAXA and CONTRAIL) data, it was found that the CO_2 sonde observation was larger than those of aircrafts by about 0.6 ppm on average. The standard deviation of the difference from the CO_2 sonde and aircraft observations was 1.2 ppm (1σ). If the 4 sets of aircraft measurement data obtained by the NIES/JAXA and CONTRAIL observations were accurate within the published uncertainties, ignoring the differences in the flight time and geographical routes, the measurement error of the CO_2 sonde system was estimated from the standard deviations of all the difference values in Tables 2 and 3. The estimated error value up to an

462 altitude of 7 km was 0.6 ± 1.2 ppm for the CO_2 sonde observation with a 240 m altitude resolution and
463 3 m s^{-1} ascending speed. The root mean square value (1.3 ppm) from all the difference value in Table
464 2 and 3 indicated that the CO_2 sonde could measure the CO_2 vertical profiles within 1.3 ppm on average
465 compared to the aircraft observations.
466
467 **c. CO_2 sonde observations over a forested area**
468 Figure **9** shows the vertical profiles of the CO_2 mole fraction, temperature, and relative humidity
469 obtained from the balloon-borne experiments of the CO_2 sonde at Moshiri (44.4°N, 142.3°E) on
470 August 26, 2009. The launch site is in a rural area of Hokkaido, Japan and is surrounded by forests.
471 The CO_2 sonde was launched at 13:29 LST and ascended with a mean vertical speed of approximately
472 3 m s^{-1}. The CO_2 sonde reached an altitude of 10 km after 56 min. The wind horizontally transported
473 the CO_2 sonde distances of 10 km and 21 km northeast when the CO_2 sonde reached the altitudes of 5
474 km and 8 km, respectively. The CO_2 sonde rapidly moved 52 km southeast at an altitude of 16 km.
475 Finally, the CO_2 sonde reached an altitude of 28 km before the balloon burst and the subsequent fall
476 of the sonde was directed by the parachute into the Sea of Okhotsk located 80 km east of the launch
477 site. The error bars for the CO_2 mole fraction in Fig. **9**a were calculated from the deviation of the signal
478 intensities from the CO_2 sensor during the 40 s measurement periods for the ambient air and the two
479 standard gases.
480 The vertical temperature profile in Fig. **9**b indicated the existence of three inversion layers of the
481 altitudes of approximately 2.0, 3.2, and 4.3 km. The relative humidity from the ground to the first
482 inversion layer at 2.0 km and between the second and third inversion layers from 3.2 to 4.3 km were
483 higher compared with those observed from 2.0 to 3.2 km and from 4.3 to 7.5 km. The CO_2 mole
484 fraction was the lowest near the ground (~373 ppm) and increased to approximately 384 ppm at an
485 altitude of 4–5 km around the third inversion layer before reaching a value of 387 ppm in the upper
486 troposphere (5–9 km). Significant decreases in the CO_2 mole fractions were observed in the two lower

layers from the ground to 3.2 km. Considering the clear weather on the day of the balloon experiment, these results are explained by the uptake of CO_2 near the surface by plants in the forests through photosynthesis processes in the daytime hours, and the diffusion and advection of the air mass containing low CO_2 concentrations in the upper altitudes.

Because the CO_2 mole fraction for the vertical profiles near the surface is critically important to estimating the flux around the observation point, the vertical profile data taken by our CO_2 sonde is useful.

d. CO_2 sonde observations over an urban area

Figure **10** shows the vertical profiles of the CO_2 mole fraction, temperature, and relative humidity obtained by the CO_2 sonde at Moriya (35.93°N, 140.00°E) on February 3rd, 2011. The launching time was 13:10 LST and the sonde ascended with a mean vertical speed of approximately 2.9 m s^{-1}. Moriya is located in the Kanto region and is 40 km northeast of the Tokyo metropolitan area. The launching site was surrounded by the heavy traffic roads and residential areas. As seen in Fig. **10**a, high CO_2 mole fractions were observed from the ground up to an altitude of 1 km. The average CO_2 volume mole fraction in this layer was higher than that measured in the free troposphere approximately above 15 ppm. A small temperature inversion layer appeared at approximately 1 km, and the maximum relative humidity was observed just below this inversion layer (Figs. **10**b and c). These results suggested that the CO_2 emitted from anthropogenic sources in and/or around the Tokyo metropolitan area accumulated in the boundary layer at altitudes below 1 km.

An analysis of Figs. **9** and **10** indicated that there were a clear local consumption and emission of CO_2 from the comparison of the levels of CO_2 concentration in the free troposphere, which suggested a decoupling with the boundary-layer and synoptic inversion layers (Mayfield and Fochesatto, 2013). When a small increase in a column XCO_2 value is observed by a satellite, it is difficult to estimate which part of the atmosphere is responsible for the increase in XCO_2, the boundary layer with strong

512 CO_2 emission in the nearby area, or the free troposphere. Considering this fact, the vertical profile data
513 obtained by the CO_2 sonde around urban areas should provide more useful information than the column
514 averaged observations obtained by the satellites and FTS measurements to estimate the flux of
515 anthropogenic CO_2 emitted in and/or around the urban areas.
516
517 **4. Conclusion**
518 The CO_2 sonde is shown to be a feasible instrument for CO_2 measurements in the troposphere. The
519 laboratory test with a vacuum chamber has shown the precision of the CO_2 sonde at ~1010 hPa for 0.6
520 ppm and at ~250 hPa for 1.2 ppm. Comparisons of the CO_2 vertical profiles obtained by the CO_2 sonde
521 with two types of aircraft observations, the CONTRAIL and the NIES/JAXA chartered aircraft, were
522 carried out. The CO_2 sonde and CONTRAIL data were consistent. The CO_2 sonde data on January
523 31st, 2011 was in good agreement with the chartered aircraft data on the same day, but the CO_2 sonde
524 data observed on February 3rd, 2011 was larger by approximately 1.4 ppm, as compared with the
525 chartered aircraft data obtained on the same day from the ground to an altitude of 7 km. The
526 measurement errors of the CO_2 sonde system up to an altitude of 7 km were estimated to be 1.4 ppm
527 for a single point of 80 s period measurements with a vertical height resolution of 240–400 m. We
528 conducted the field CO_2 sonde observations more than 20 times in Japan and successfully obtained
529 CO_2 vertical profiles from the ground up to altitudes of approximately 10 km.
530 Our results showed that low-cost CO_2 sondes could potentially be used for frequently measurements
531 of vertical profiles of CO_2 in any parts of the world providing as useful information to understand the
532 global and regional carbon budgets by replenishing the present sparse observation coverage. The CO_2
533 sondes can detect the local and regional transport evidence by determining CO_2 concentrations in the
534 air layer trapped between elevated inversion layers. Also, the CO_2 sonde observation data will help
535 improve the inter-comparison exercise for inverse models and for the partial validation of satellite
536 column integral data. In future, the CO_2 sonde data will be used for the validation of satellites and the

calibration of ground-based observations of sunlight spectroscopic measurements for column values of CO_2 concentration.

Acknowledgments

We would like to thank N. Toriyama, M. Kanada, H. Jindo, M. Sera, H. Sasago, T. Ide, S. Takekawa, M. Kawasaki, G. Inoue (Nagoya Univ.), M. Fujiwara, Y. Inai (Hokkaido Univ.), S. Aoki, and T. Nakazawa (Tohoku Univ.) for their assistance and useful suggestions in the development of CO_2 sonde and the observations. This work was partly supported by the Grant-in-Aid for Scientific Research (KAKENHI 20310008 and 24310012), Green Network of Excellence, Environmental Information (GRENE-ei) program from the Ministry of Education, Culture, Sports, Science and Technology (MEXT), Development of Systems and Technology for Advanced Measurement and Analysis Program from Japan Science and Technology Agency (JST), and the joint research program of the Solar-Terrestrial Environment Laboratory (Now new organization: the Institute for Space-Earth Environmental Research), Nagoya University.

553 **References**

554 Ahmadov, R., Gerbig, C., Kretschmer, R., Körner, S., Rödenbeck, C., Bousquet, P., and Ramonet,
555 M.: Comparing high resolution WRF-VPRM simulation and two global CO_2 transport models
556 with coastal tower measurements of CO_2, Biogeosciences, **6**, 807–817, doi:10.5194/bg-6-807-
557 2009, 2009.
558 Andrews, A. E. and Coauthors: CO_2, CO, and CH_4 measurements from tall towers in the NOAA
559 Earth System Research Laboratory's Global Greenhouse Gas Reference Network:
560 instrumentation, uncertainty analysis, and recommendations for future high-accuracy greenhouse
561 gas monitoring efforts, Atmos. Meas. Tech., **7**, 647-687, doi:10.5194/amt-7-647-2014, 2014.
562 Baker, D. F. and Coauthors: TransCom 3 inversion intercomparison: Impact of transport model errors
563 on the interannual variability of regional CO_2 fluxes, 1988–2003, Global Biogeochem. Cycles, **20**,
564 GB1002, doi:10.1029/2004GB002439, 2006.
565 Bakwin, P. S., Tans, P. P., Zhao, C., Ussler III, W., and Quesnell, E.: Measurements of carbon dioxide
566 on a very tall tower, Tellus **47B**, 535-549, 1995, doi:10.1034/j.1600-0889.47.issue5.2.x, 2002.
567 Chédin, A., Serrar, S., Armante, R., Scott, N. A., and Hollingsworth, A.: Signatures of annual and
568 seasonal variations of CO_2 and other greenhouse gases from comparisons between NOAA TOVS
569 observations and radiation model simulations, J. Climate, **15**, 95-116, doi:10.1175/1520-
570 0442(2002)015<0095:SOAASV>2.0.CO;2, 2002.
571 Conway, T. J., Tans, P. P., Waterman, L. S., Thoning, K. W., Masarie, K. A., and Gammon, R. H.:
572 Atmospheric carbon dioxide measurements in the remote global troposphere, 1981–1984, *Tellus*
573 *B*, **40**, 81–115, doi:10.1111/j.1600-0889.1988.tb00214.x., 1988.
574 Conway, T. J., Tans, P. P., Waterman, L. S., Thoning, K. W., Kitzis, D. R., Masarie, K. A. and Zhang,
575 N.: Evidence for interannual variability of the carbon cycle from the National Oceanic and
576 Atmospheric Administration/Climate Monitoring and Diagnostics Laboratory global air sampling
577 network, J. Geophys. Res., **99**(D11), 22,831–22,855, doi:10.1029/94JD01951, 1994.

578 Crevoisier, C., Heilliette, S., Chédin, A., Serrar, S., Armante, R. and Scott, N. A.: Midtropospheric
579 CO_2 concentration retrieval from AIRS observations in the tropics, Geophys. Res. Let., **31**,
580 L17106, doi:10.1029/2004GL020141, 2004.
581 Daube, B. C., Boering, K. A., Andrews, A. E. and Wofsy, S. C.: A high-precision fast-response
582 airborne CO_2 analyzer for in situ sampling from the surface to the middle stratosphere, J.
583 Atmospheric Ocean. Technol., **19**(10), 1532-1543, doi:10.1175/1520-0426(2002)019
584 <1532:AHPFRA>2.0.CO;2, 2002.
585 Dils, B. and Coauthors: Comparisons between SCIAMACHY and ground-based FTIR data for total
586 columns of CO, CH_4, CO_2 and N_2O, *Atmos. Chem. Phys.,* **6**, 1953–1976, doi:10.5194/acp-6-1953-
587 2006, 2006.
588 Durry, G., Amarouche, N., Zéninari, V., Parvitte, B., Lebarbu, T. and Ovarlez, J.: In situ sensing of
589 the middle atmosphere with balloon borne near-infrared laser diodes, Spectrochimica Acta Part A,
590 **60**, 3371–3379, doi:10.1016/j.saa.2003.11.050, 2004.
591 Eldering, A. and Coauthors: The Orbiting Carbon Observatory-2: first 18 months of science data
592 products, Atmos. Meas. Tech., **10**, 549-563, doi:10.5194/amt-10-549-2017, 2017.
593 Fang, S. X., Zhou, L. X., Tans, P. P., Ciais, P., Steinbacher, M., Xu, L., and Luan, T.: In situ
594 measurement of atmospheric CO_2 at the four WMO/GAW stations in China, *Atmos. Chem. Phys.*,
595 14, 2541–2554, doi:10.5194/acp-14-2541-2014, 2014.
596 Gurney, K. R. and Coauthors: Towards robust regional estimates of CO_2 sources and sinks using
597 atmospheric transport models, Nature, **415**, 626-630, doi:10.1038/415626a, 2002.
598 Gurney, K. R. and Coauthors: Transcom 3 inversion intercomparison: Model mean results for the
599 estimation of seasonal carbon sources and sinks. Global Biogeochem. Cycles, **18**, GB1010,
600 doi:10.1029/2003GB002111, 2004.
601 Ghysels, M., Durry, G., Amarouche, N., Cousin, J., Joly, L., Riviere, E. D., and Beaumont, L.: A
602 lightweight balloon-borne laser diode sensor for the in situ measurement of CO_2 at 2.68 micron in

603 the upper troposphere and the lower stratosphere, Appl. Phys. B, **107**(1), 213-220,
604 doi:10.1007/s00340-012-4887-y, 2012.
605 Hodgkinson, J., Smith, R., Ho, Wah On, Saffell, J. R.. Tatam, R. P.: Non-dispersive infra-red (NDIR)
606 measurement of carbon dioxide at 4.2 μm in a compact and optically efficient sensor, Sensors and
607 Actuators B, **186**, 580– 588. doi: 10.1016/j.snb.2013.06.006, 2013.
608 Inai Y., Aoki, S., Honda, H., Furutani, H., Matsumi, Y., Ouchi, M., Sugawara, S., Hasebe, F.,
609 Uematsu, M., Fujiwara, M.: Balloon-borne tropospheric CO_2 observations over the equatorial
610 eastern and western Pacific, Atmos. Env., **184**, 24-36. doi: 10.1016/j.atmosenv.2018.04.016, 2018.
611 Inoue, H. Y., and Matsueda, H.: Measurements of atmospheric CO_2 from a meteorological tower in
612 Tsukuba, Japan. Tellus, **53B**, 205–219, doi:10.1034/j.1600-0889.2001.01163.x, 2001.
613 Joly. L., Parvitte, B., Zeninari, V. and Durry, G.: Development of a compact CO_2 sensor open to the
614 atmosphere and based on near-infrared laser technology at 2.68 μm, Appl. Phys. B, **86**, 743–748,
615 doi:10.1007/s00340-006-2568-4, 2007.
616 Karion, A., C. Sweeney, P. Tans, and T. Newberger, 2010: AirCore: An innovative atmospheric
617 sampling system, *J. Atmos. Oceanic Technol.,* **27**, 1839–1853, doi:10.1175/2010JTECHA1448.1.
618 Komhyr, W. D., Harris, T. B., Waterman, L. S., Chin, J. F. S. and Thoning, K. W.: Atmospheric
619 carbon dioxide at Mauna Loa Observatory 1. NOAA global monitoring for climatic change
620 measurements with a nondispersive infrared analyzer, 1974–1985, J. Geophys. Res., **94**, 8533–
621 8547, doi:10.1029/JD094iD06p08533, 1989.
622 Machida, T., Matsueda, H., Sawa, Y., Nakagawa, Y., Hirotani, K., Kondo, N., Goto, K., Ishikawa, K.,
623 Nakazawa, T., and Ogawa, T.: Worldwide measurements of atmospheric CO_2 and other trace gas
624 species using commercial airlines, J. Atmos. Oceanic Technol., **25**(10), 1744–1754,
625 doi:10.1175/2008JTECHA1082.1, 2008.
626 Maksyutov, S., Nikolay, K., Nakatsuka, Y., Patra, P. K., Nakazawa, T., Yokota, T., and Inoue, G.:
627 Projected Impact of the GOSAT observations on regional CO_2 flux estimations as a function of

628 total retrieval error. J. Remote Sensing Soc. Japan, **28**, 190-197, doi:10.11440/rssj.28.190, 2008.
629 Matsueda, H., Machida, T., Sawa, Y., Nakagawa, Y., Hirotani, K., Ikeda, H., Kondo, N., and Goto,
630 K.: Evaluation of atmospheric CO_2 measurements from new flask air sampling of JAL airliner
631 observations. *Pap. Meteor. Geophys.*, **59**, 1–17, doi:10.2467/mripapers.59.1, 2008.
632 Mayfield J. A. and Fochesatto, G. J.: The Layered Structure of the winter Atmospheric Boundary Layer in the
633 Interior of Alaska. J. Appl. Met. Climatol., 52, 953-973, doi.org/10.1007/s00703-013-0274-4, 2013.
634 Morino, I. and Coauthors, 2011: Preliminary validation of column-averaged volume mixing ratios of
635 carbon dioxide and methane retrieved from GOSAT short-wavelength infrared spectra, Atmos.
636 Meas. Tech., **4**, 1061–1076, doi:10.5194/amt-4-1061-2011.
637 Nakazawa, T., Murayama, S., Miyashita, K., Aoki, S., and Tanaka, M.: Longitudinally different
638 variations of lower tropospheric carbon dioxide concentrations over the North Pacific Ocean,
639 Tellus, **44B**, 161–172, doi:10.3402/tellusb.v44i3.15438, 1992
640 Nakazawa, T., Machida, T., Sugawara, S., Murayama, S., Morimoto, S., Hashida, G., Honda, H. and
641 Itoh, T.: Measurements of the stratospheric carbon dioxide concentration over Japan using a
642 balloon-borne cryogenic sampler, Geophys. Res. Letter, **22**, 1229–1232, doi:10.1029/95GL0118,
643 1995.
644 Pales, J. C., and Keeling, C. D.: The concentration of atmospheric carbon dioxide in Hawaii, J.
645 Geophys. Res., **70**(24), 6053-6076, doi:10.1029/JZ070i024p06053, 1965.
646 Stephens, B. B. and Coauthors: Weak northern and strong tropical land carbon uptake from vertical
647 profiles of atmospheric CO_2, Science, **316**, 1732–1735, doi:10.1126/science.1137004, 2007.
648 Sweeney, C. and Coauthors: Seasonal climatology of CO_2 across North America from aircraft
649 measurements in the NOAA/ESRL Global Greenhouse Gas Reference Network, J. Geophys. Res.,
650 **120**, 5155-5190, doi:10.1002/2014JD022591, 2014.
651 Tanaka, M., Nakazawa, T. and Aoki, S.: High quality measurements of the concentration of
652 atmospheric carbon dioxide. *J. Meteor. Soc. Japan*, **61**, 678-685, doi:10.2151/jmsj1965.61.4_678,

1983.

Tanaka, M., Nakazawa, T. and Aoki S.: Time and space variations of tropospheric carbon dioxide over Japan, Tellus, **39B**, 3–12, doi:10.3402/tellusb.v39i1-2.15318, 1987.

Tanaka, T., Miyamoto, Y., Morino, I., Machida, T., Nagahama, T., Sawa, Y., Matsueda, H., Wunch, D., Kawakami, S., and Uchino, O.: Aircraft measurements of carbon dioxide and methane for the calibration of ground-based high-resolution Fourier Transform Spectrometers and a comparison to GOSAT data measured over Tsukuba and Moshiri. Atmos. Meas. Tech., **5**, 2003–2012, doi:10.5194/amt-5-2003-2012, 2012.

Tans, P. P., Conway, T., and Nakazawa T.: Latitudinal distribution of the sources and sinks of atmospheric carbon dioxide derived from surface observations and an Atmospheric Transport Model, J. Geophys. Res., **94**, 5151–5172, doi:10.1029/JD094iD04p05151, 1989.

Watai, T., Machida, T., Ishizaki, N. and Inoue, G.: A lightweight observation system for atmospheric carbon dioxide concentration using a small unmanned aerial vehicle, J. Atmos. Oceanic Technol., **23**, 700–710 doi:10.1175/JTECH1866.1, 2006.

Winderlich, J., Chen, H., Gerbig, C., Seifert, T., Kolle, O., Lavrič, J. V., Kaiser, C., Höfer, A., and Heimann, M.: Continuous low-maintenance CO_2/CH_4/H_2O measurements at the Zotino Tall Tower Observatory (ZOTTO) in Central Siberia, Atmos. Meas. Tech., **3**, 1113–1128, doi:10.5194/amt-3-1113-2010, 2010.

WMO: The state of greenhouse gases in the atmosphere using global observations through 2015, WMO Greenhouse Gas Bull., **12**, 1–8, 2016.

Wofsy, S. C., the HIPPO science team and cooperating modellers and satellite teams: HIAPER Pole-to-Pole Observations (HIPPO): fine-grained, global-scale measurements of climatically important atmospheric gases and aerosols, *Phil. Trans. R. Soc. A*, **369**, 2073–2086, doi:10.1098/rsta.2010.0313, 2011.

Wunch, D., Toon, G. C., Blavier, J. L., Washenfelder, R. A., Notholt, J., Connor, B. J., Griffith, D. W.

678 T., Sherlock, V. and Wennberg, P. O.: The Total Carbon Column Observing Network. Phil. Trans.
679 R. Soc. A, **369**, 2087–2112, doi:10.1098/rsta.2010.0240, 2011.
680 Yokota, T., Yoshida, Y., Eguchi, N., Ota, Y., Tanaka, T., Watanabe, H. and Maksyutov, S.: Global
681 concentrations of CO_2 and CH_4 retrieved from GOSAT: First preliminary results, Sci. Online Lett.
682 Atmos., **5**, 160–163, doi:10.2151/sola.2009–041, 2009.
683 Yoshida, Y., Ota, Y., Eguchi, N., Kikuchi, N., Nobuta, K., Tran, H., Morino, I., and Yokota, T.:
684 Retrieval algorithm for CO_2 and CH_4 column abundances from short-wavelength infrared spectral
685 observations by the Greenhouse gases observing satellite, Atmos. Meas. Tech., **4**, 717–734,
686 doi:10.5194/amt-4-717-2011, 2011.
687

688 **Table 1**. CONTAIL flight data near to the CO_2 sonde measurements on 31 January and 3 February

689 2011.

690

691

Data set name	Date	Time (LST)[a]
11_057a	CONTRAIL (29 January)	19:01
11_058d	CONTRAIL (30 January)	15:06
11_059a	CONTRAIL (30 January)	18:46
11_060d	CONTRAIL (31 January)	15:07
11_061a	CONTRAIL (1 February)	18:46
11_062d	CONTRAIL (2 February)	14:58
11_063a	CONTRAIL (4 February)	18:58
	CO_2 sonde (31 January)	13:06
	CO_2 sonde (3 February)	13:10

692

693 [a] Time for the CONTRAIL data represents the flight time in Japan Standard Time at an altitude of 1

694 km over the Narita airport. Time for the CO_2 sonde data represents the launching time at Moriya.

695

696

697

Table 2. Comparisons of the CO_2 concentrations between the balloon CO_2 sonde and NIES/JAXA chartered aircraft measurements on 31st January and 3rd February 2011.

JAXA-NIES Chartered Aircraft (31 January 2011)						JAXA-NIES Chartered Aircraft (3 February 2011)			
Altitude (m)[a]	Balloon CO_2 (ppm) spline[b]	Balloon CO_2 (ppm) linear[c]	Aircraft CO_2 (ppm)[d]	Difference (ppm) spline[e]	Difference (ppm) linear[f]	Altitude (m)[a]	Balloon CO_2 (ppm) spline[b]	Aircraft CO_2 (ppm)[d]	Difference (ppm) spline[e]
849	399.05	400.92	397.62	1.43	3.30	1324	396.60	394.45	2.15
1202	398.16	399.58	397.53	0.63	2.05	1612	394.65	393.03	1.62
1610	398.00	399.99	397.17	0.83	2.82	1917	394.86	394.10	0.76
2038	396.50	401.35	396.95	-0.45	4.40	2223	395.77	393.54	2.23
2291	398.03	401.83	396.04	1.99	5.79	2539	395.41	393.95	1.45
2463	396.54	396.45	395.65	0.89	0.80	2867	394.71	395.11	-0.40
2844	393.44	394.15	395.24	-1.79	-1.09	3215	394.99	392.99	2.00
3329	395.45	398.68	394.15	1.30	4.53	3543	393.59	393.07	0.52
3732	393.51	396.87	393.63	-0.12	3.24	3764	393.69	393.40	0.28
4161	395.47	396.99	393.54	1.93	3.45	3938	395.15	393.11	2.04
4575	394.62	396.38	392.94	1.68	3.44	4169	393.83	392.68	1.15
4918	393.24	396.00	393.64	-0.41	2.36	4458	396.57	393.51	3.06
5273	392.41	395.02	393.25	-0.84	1.77	4750	394.88	393.69	1.19
5654	393.02	395.31	393.47	-0.45	1.84	5047	396.53	394.01	2.53
6083	391.87	395.19	392.91	-1.04	2.28	5214	395.91	393.45	2.46
6510	392.76	395.44	391.65	1.11	3.79	5383	396.78	393.58	3.20
			Average =	0.42	2.80	5565	395.83	393.67	2.15
			Std Dev[g] =	1.16	1.61	5781	395.18	393.39	1.80
			RMS[h] =	1.20	1.62	6092	391.75	392.83	-1.09
						6287	392.44	392.42	0.02
						6467	393.67	392.23	1.44
						6639	395.07	392.42	2.65
						6815	394.00	393.00	1.00
								Average =	1.41
								Std Dev[d] =	1.00
								RMS[e] =	1.62

a. Altitudes of the balloon-borne experiments using the in-flight calibration with 40-s time intervals.

b. Balloon measurement results calculated using the cubic spline fitting method.

c. Balloon measurement results calculated using the linear fitting method.

d. Averaged values of the aircraft measurement results over the range of the balloon altitudes ± 100 m.

e. Difference values of [balloon CO_2](cubic spline fitting) - [Aircraft CO_2]

f. Difference values of [balloon CO_2] (linear fitting)- [Aircraft CO_2]

g. Standard deviation of the differences (1σ).

h. Root mean square values. **Table 3.** Comparisons of the CO_2 concentrations between the balloon CO_2 sonde measurements on 31 January and CONTRAIL aircraft CME on 31 January (11_060d) and between the CO_2 sonde on 3 February and CONTRAIL on 2 February (11_062d) up to the altitude of 7 km. The annotations are same as Table 2.

CONTRAIL 11_060d (31 January 2011)				CONTRAIL 11_062d (2 February 2011)			
Altitude (m)	Balloon CO_2 (ppm)	Aircraft CO_2 (ppm)	Difference (ppm)	Altitude (m)	Balloon CO_2 (ppm)	Aircraft CO_2 (ppm)	Difference (ppm)
849	399.05	398.21	0.84	1917	394.86	396.59	-1.73
1202	398.16	399.56	-1.40	2223	395.77	396.45	-0.68
1610	398.00	398.77	-0.76	2539	395.41	395.71	-0.30
2038	396.50	397.07	-0.57	2867	394.71	394.67	0.04
2291	398.03	395.97	2.06	3215	394.99	393.34	1.65
2463	396.54	394.55	1.99	3543	393.59	394.25	-0.66
2844	393.44	393.41	0.04	3764	393.69	394.33	-0.64
3329	395.45	394.25	1.20	3938	395.15	394.69	0.46
3732	393.51	393.58	-0.07	4458	396.57	394.09	2.48
4161	395.47	393.86	1.61	4750	394.88	395.02	-0.14
4575	394.62	393.18	1.44	5047	396.53	396.55	-0.01
4918	393.24	393.62	-0.38	5214	395.91	396.01	-0.10
5273	392.41	392.76	-0.35	5383	396.78	394.78	2.00
6866	392.31	393.26	-0.96	5565	395.83	393.69	2.14
		Average =	0.33	5781	395.18	393.79	1.39
		Std Dev =	1.16	6092	391.75	393.57	-1.82
		RMS =	1.17	6287	392.44	393.32	-0.88
				6467	393.67	392.89	0.78
				6639	395.07	392.84	2.23
				6815	394.00	393.11	0.90
						Average =	0.35
						Std Dev =	1.30
						RMS =	1.31

715 **Figure captions**

716 **Figure 1.** Left: Schematic diagram of the CO_2 measurement package, where F1 and F2 represent the
717 band-pass filters at wavelengths of 4.0 μm and 4.3 μm, respectively. The outlet port of the CO_2 sensor
718 is opened to ambient air. Details of the system are described in the text. Right: Photograph of the inside
719 of the CO_2 sonde package. The components were placed in a specially modeled expanded polystyrene
720 box.

721 **Figure 2**. Photograph of the CO_2 sonde developed in this study before launching. a. CO_2
722 measurement package is shown in Fig. **1**, b. GPS sonde, and c. Calibration gas package.

723 **Figure 3**. Raw data obtained by the CO_2 sonde launched on September 26, 2011 at Moriya, Japan. The
724 vertical axis is the difference between the 4.0 μm and 4.3 μm signal intensities divided by the ambient
725 pressure. The black line indicates the observation results during the balloon flight with calibration
726 cycles. The red circle indicates the 30 s average values in each step of the calibration. Red curve
727 indicates the cubic spline fitting curves for the observation points of the 30 s average values of the
728 same standard gas. The small black dots on the cubic spline curves indicate the estimated values for
729 the standard gases at the ambient gas measuring timing, which were is used for the interpolation to
730 determine the ambient air concentrations.

731 **Figure 4.** $[I(4.0) - I(4.3)]/P$ values versus CO_2 mole fraction, where $I(4.0)$ and $I(4.3)$ are the
732 signal intensities at the 4.0 μm wavelength for background measurements and the 4.3 μm wavelength
733 for CO_2 absorption measurements, obtained by the NDIR CO_2 sensor, and P is the ambient
734 atmospheric pressure. CO_2 mole fractions were measured with a standard NDIR instrument (LICOR,
735 LI-840A) connected to the balloon sensor in series. The pressure while carrying out the
736 measurements was constant at 1010 hPa.

737 **Figure 5**. Results of a chamber experiment of the CO_2 sonde. Pressure in the chamber was reduced
738 from 1010 hPa (ground level pressure) to 250 hPa (about 10 km altitude pressure) at a temperature of
739 about 298 K. The black circles indicate the value of the CO_2 mole fraction of the sample air in the

chamber, which was obtained from the interpolation of the standard gas values in each calibration cycle. Vertical error bars indicate the square-root of sum of squares for the standard deviations of the sample and standard gas signals at each step in the calibration cycle. The black dashed line shows an average of all the values obtained for the sample gas. See the text for more details.

Figure 6. Flight paths of the CO_2 sonde observations launched at Moriya on January 31st (blue solid line) and February 3rd (red solid line), 2011, the CONTRAIL 11_060d data on January 31st, 2011 (black solid line) and 11_062d data on February 2nd, 2011 (black dashed line) from Hong Kong to Narita, and the NIES/JAXA chartered aircraft experiment on January 31st (green solid line) and February 3rd (purple dotted line). The altitudes of the flight paths are also indicated.

Figure 7. The CO_2 vertical profiles obtained by the CO_2 sonde (circles connected with blue lines), NIES/JAXA chartered aircraft data (dots connected with green lines), and the CONTRAIL data (diamonds connected with black lines) on January 31st, 2011.

Figure 8. The CO_2 vertical profiles obtained by the CO_2 sonde (circles connected with red lines), NIES/JAXA chartered aircraft data (dots connected with purple lines) on February 3rd, and CONTRAIL data (diamonds connected with black lines) on February 2nd, 2011.

Figure 9. Profiles of (a) CO_2 mole fraction, (b) temperature (solid line) and potential temperature (dotted line), and (c) relative humidity (Solid line, %) and water mol fraction (dotted line, unit 1/5000 mol/mol) observed over a forest area, Moshiri in Hokkaido, Japan by the balloon launched on August 26, 2009 at 13:30 (LST). The black circles with error bars in panel (a) represent the data obtained by the CO_2 sonde.

Figure 10. Profiles of (a) CO_2 mole fraction, (b) temperature (solid line) and potential temperature (dotted line), and (c) relative humidity (Solid line, %) and water mol fraction (dotted line, unit 1/5000 mol/mol) observed over an urban area, Moriya near Tokyo on February 3rd, 2011 at 13:10 (LST).

765

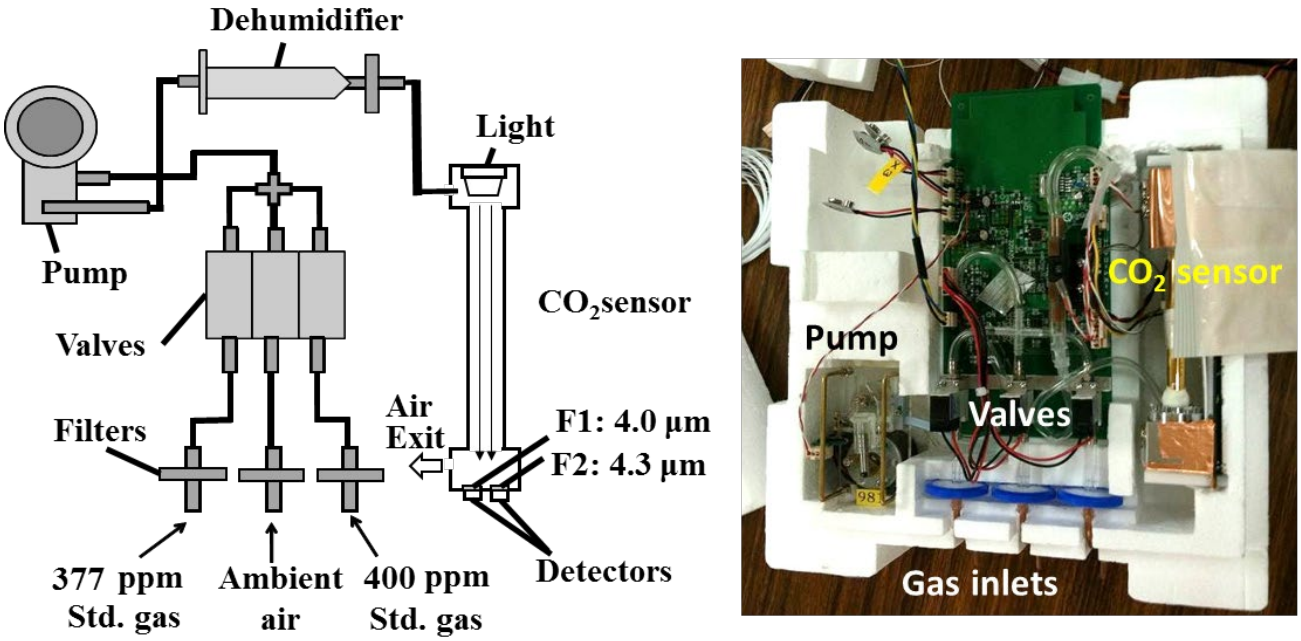

766

767 **Figure 1.** Left: Schematic diagram of the CO_2 measurement package, where F1 and F2 represent the
768 band-pass filters at wavelengths of 4.0 µm and 4.3 µm, respectively. The outlet port of the CO_2 sensor
769 is opened to ambient air. Details of the system are described in the text. Right: Photograph of the inside
770 of the CO_2 sonde package. The components were placed in a specially modeled expanded polystyrene
771 box.

772

773

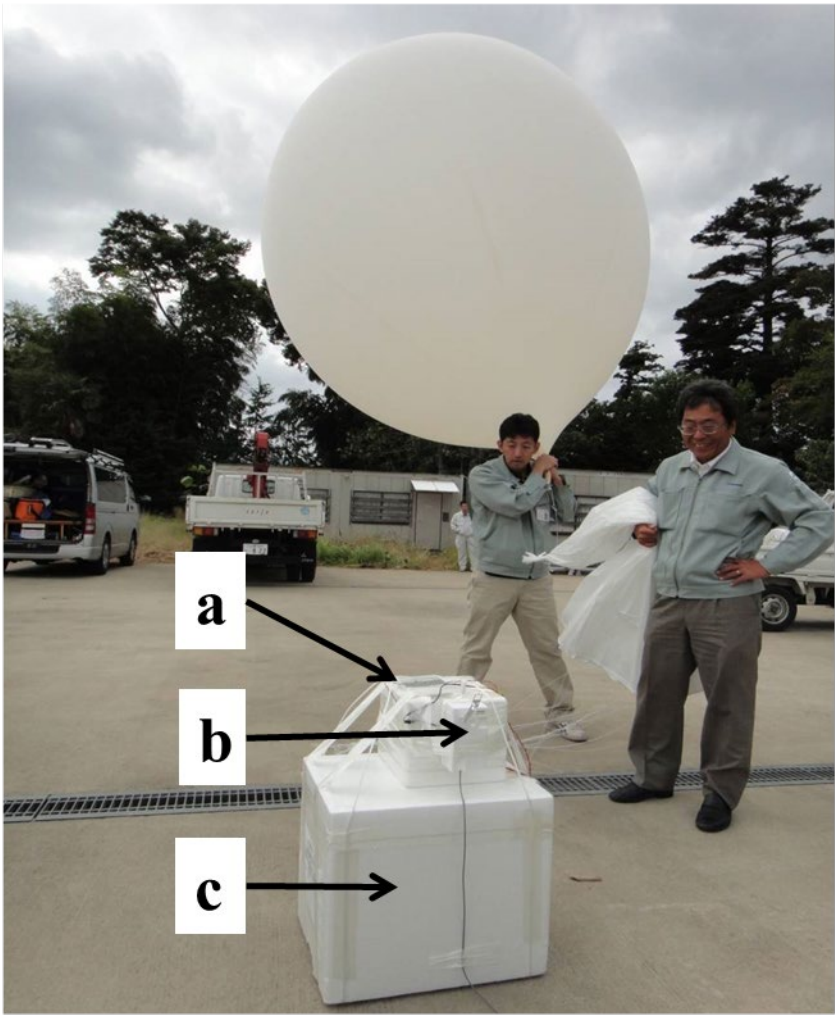

774

775 **Figure 2**. Photograph of the CO_2 sonde developed in this study before launching. a. CO_2

776 measurement package is shown in Fig. **1**, b. GPS sonde, and c. Calibration gas package.

777

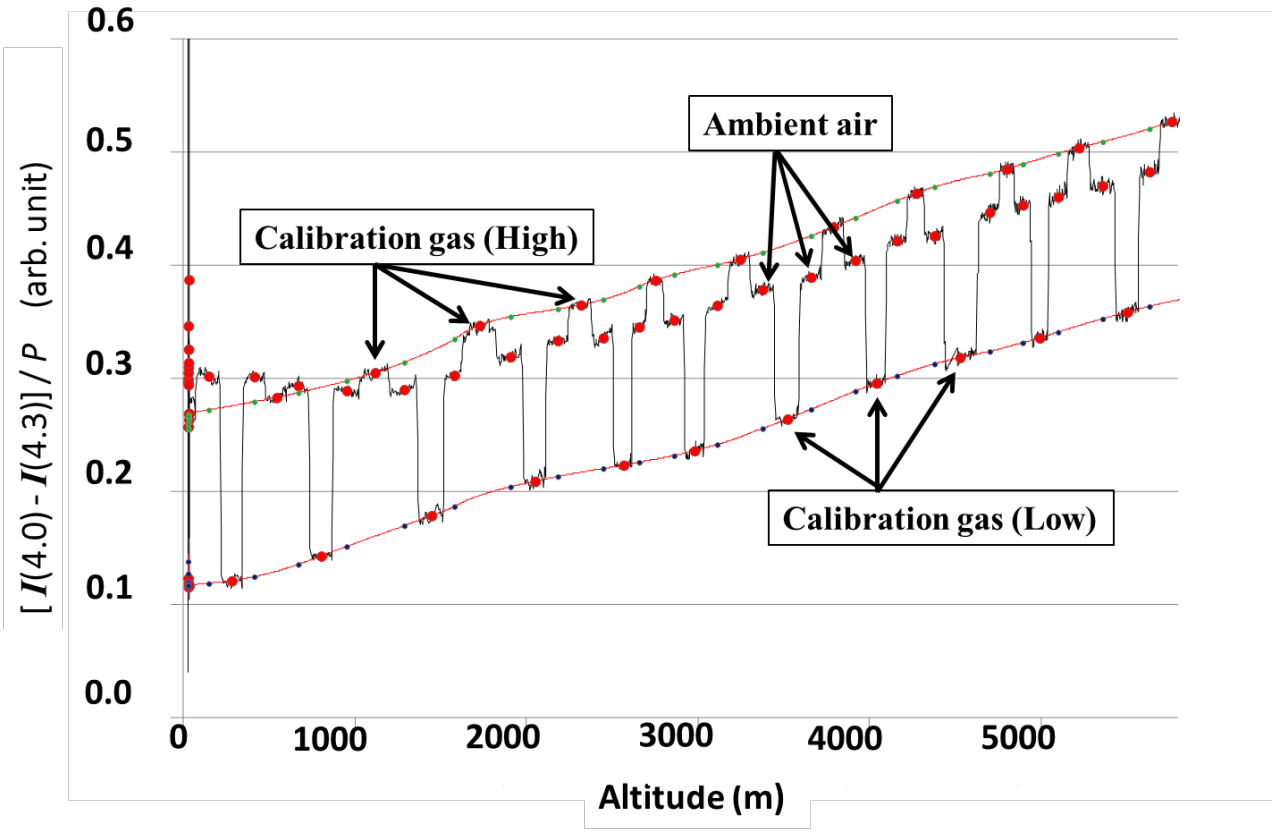

778 **Figure 3**. Raw data obtained by the CO_2 sonde launched on September 26, 2011 at Moriya, Japan.
779 The vertical axis is the difference between the 4.0 μm and 4.3 μm signal intensities divided by the
780 ambient pressure. The black line indicates the observation results during the balloon flight with
781 calibration cycles. The red circle indicates the 30 s average values in each step of the calibration. Red
782 curve indicates the cubic spline fitting curves for the observation points of the 30 s average values of
783 the same standard gas. The small black dots on the cubic spline curves indicate the estimated values
784 for the standard gases at the ambient gas measuring timing, which were is used for the interpolation
785 to determine the ambient air concentrations.
786
787

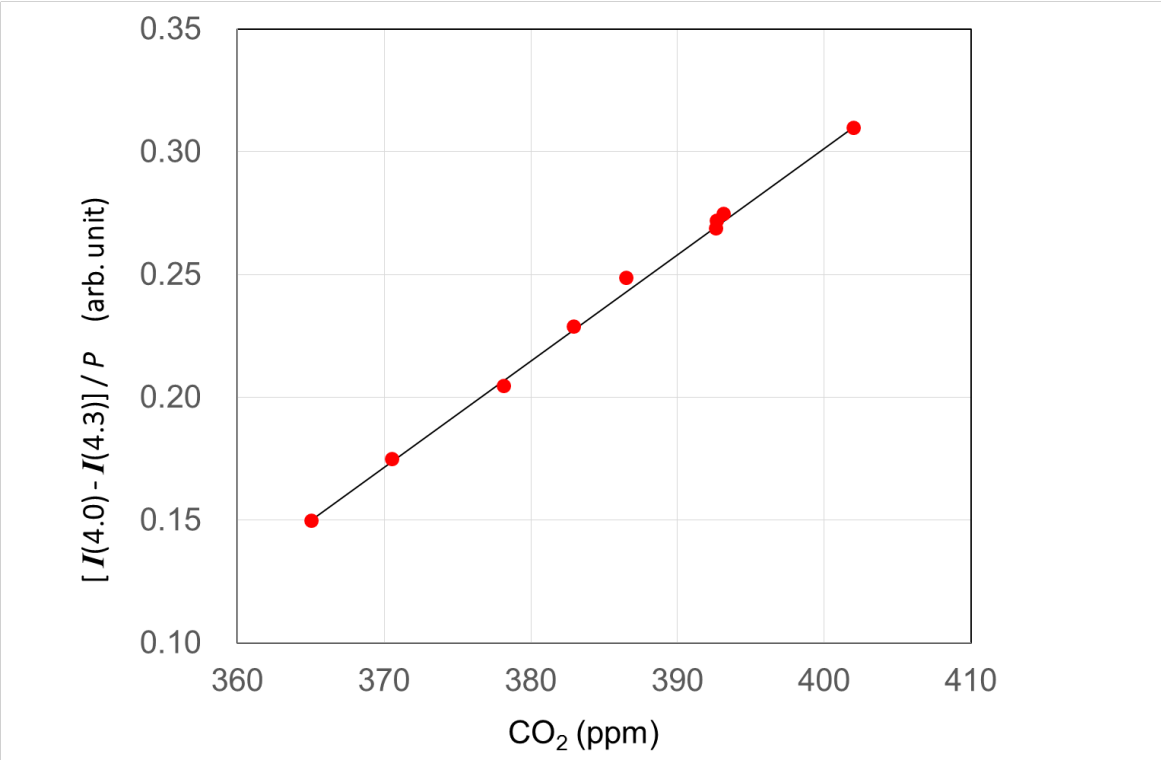

Figure 4. $[I(4.0)-I(4.3)]/P$ values versus CO_2 mole fraction, where $I(4.0)$ and $I(4.3)$ are the signal intensities at the 4.0 μm wavelength for background measurements and the 4.3 μm wavelength for CO_2 absorption measurements, obtained by the NDIR CO_2 sensor, and P is the ambient atmospheric pressure. CO_2 mole fractions were measured with a standard NDIR instrument (LICOR, LI-840A) connected to the balloon sensor in series. The pressure while carrying out the measurements was constant at 1010 hPa.

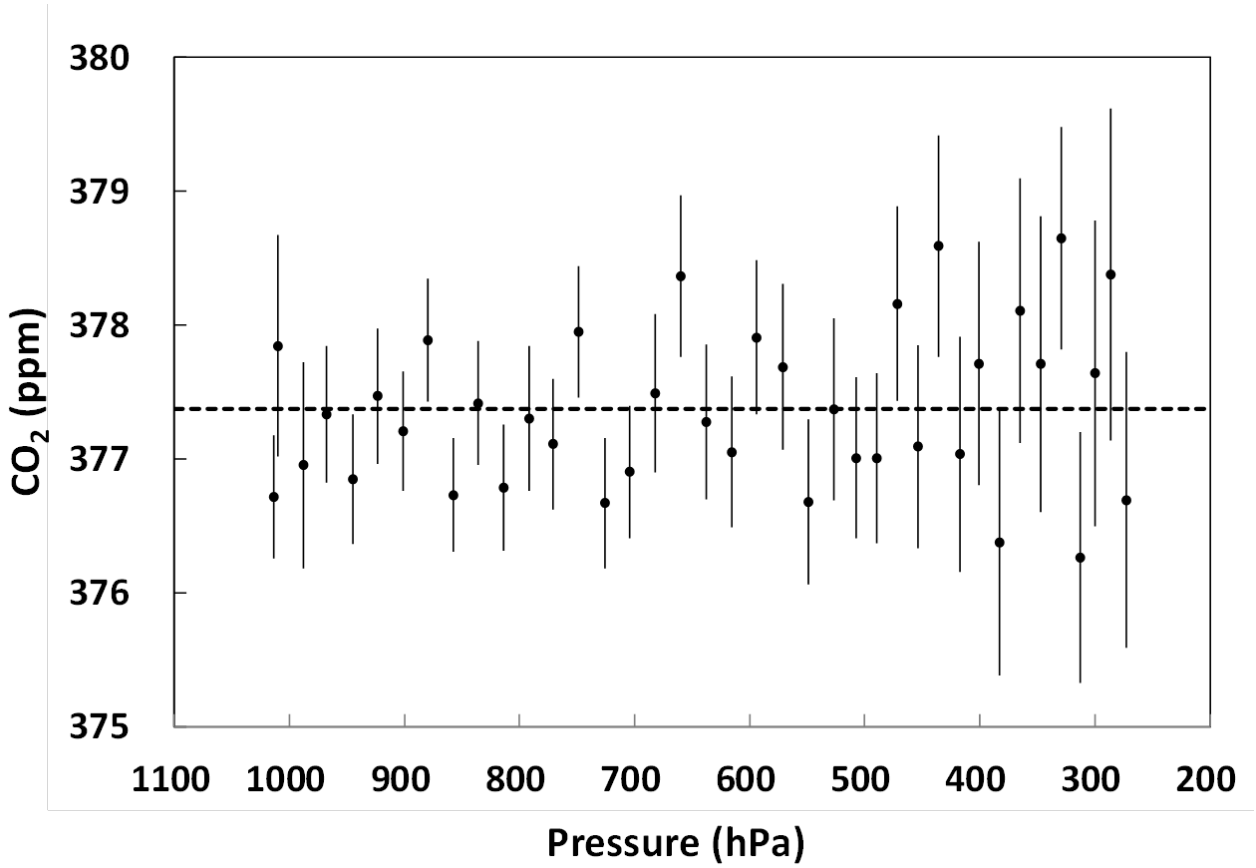

798

799

800 **Figure 5**. Results of a chamber experiment of the CO_2 sonde. Pressure in the chamber was reduced
801 from 1010 hPa (ground level pressure) to 250 hPa (about 10 km altitude pressure) at a temperature of
802 about 298 K. The black circles indicate the value of the CO_2 mole fraction of the sample air in the
803 chamber, which was obtained from the interpolation of the standard gas values in each calibration
804 cycle. Vertical error bars indicate the square-root of sum of squares for the standard deviations of
805 the sample and standard gas signals at each step in the calibration cycle. The black dashed line shows
806 an average of all the values obtained for the sample gas. See the text for more details.

807

808

809

810

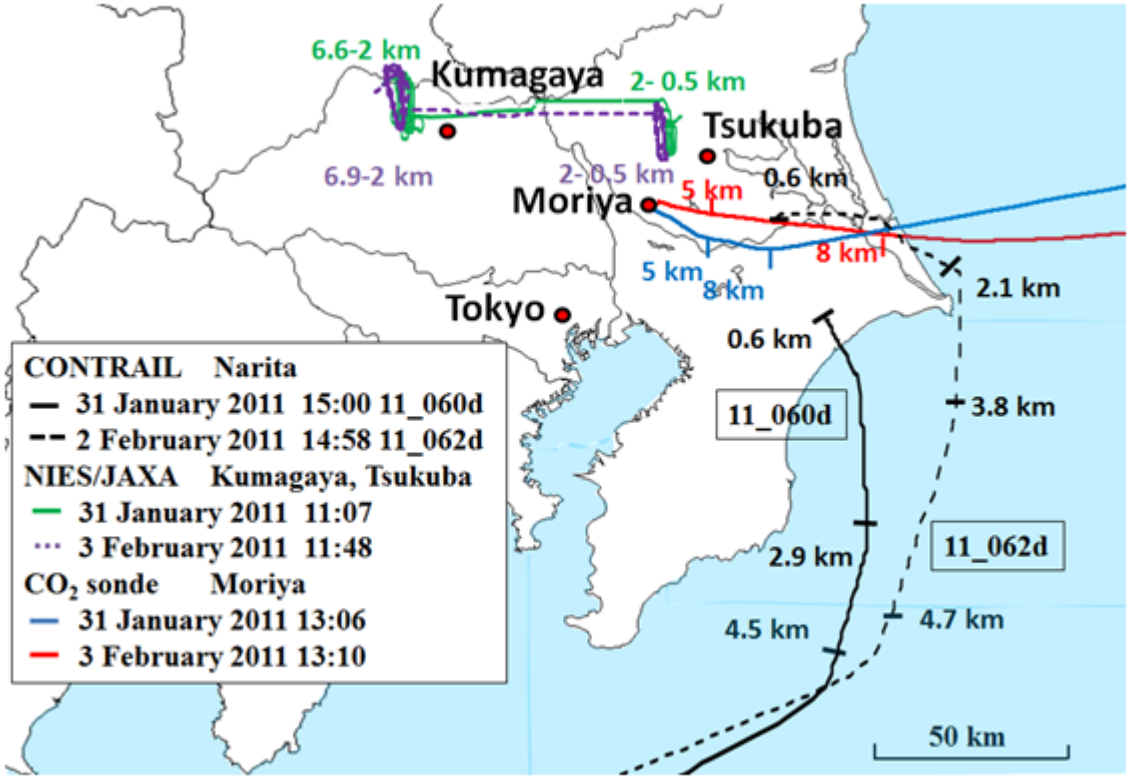

811

812

813 **Figure 6**. Flight paths of the CO_2 sonde observations launched at Moriya on January 31st (blue solid
814 line) and February 3rd (red solid line), 2011, the CONTRAIL 11_060d data on January 31st, 2011
815 (black solid line) and 11_062d data on February 2nd, 2011 (black dashed line) from Hong Kong to
816 Narita, and the NIES/JAXA chartered aircraft experiment on January 31st (green solid line) and
817 February 3rd (purple dotted line). The altitudes of the flight paths are also indicated.

818

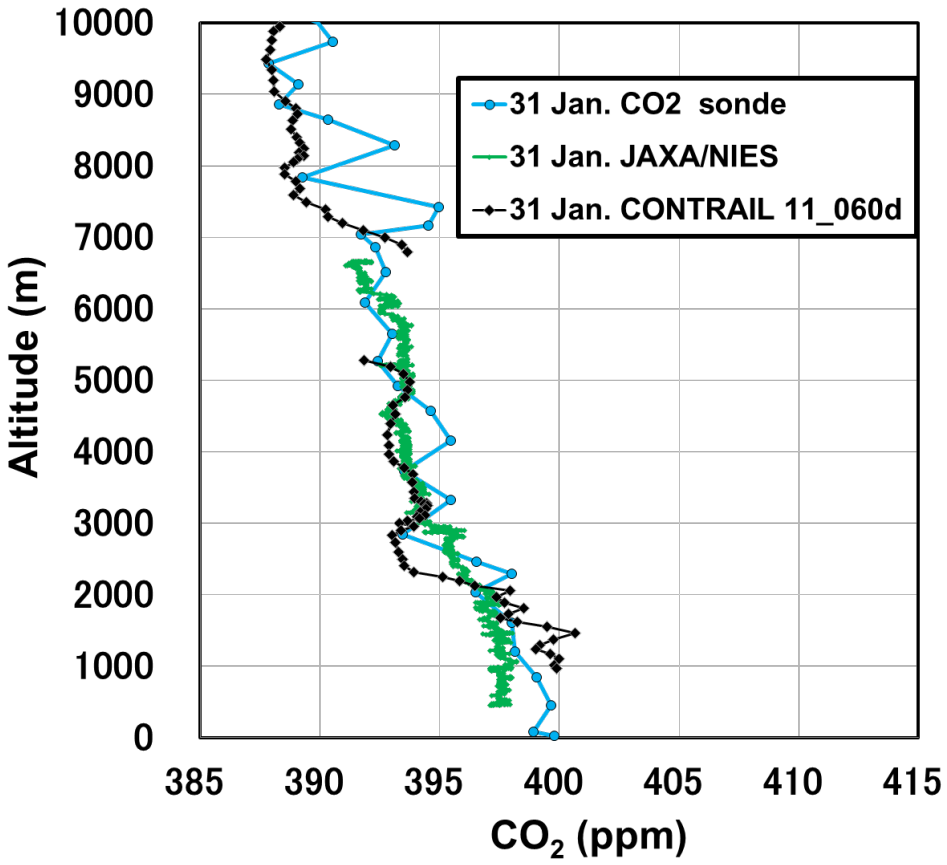

819

820 **Figure 7**. The CO_2 vertical profiles obtained by the CO_2 sonde (circles connected with blue lines),
821 NIES/JAXA chartered aircraft data (dots connected with green lines), and the CONTRAIL data
822 (diamonds connected with black lines) on January 31st, 2011.

823

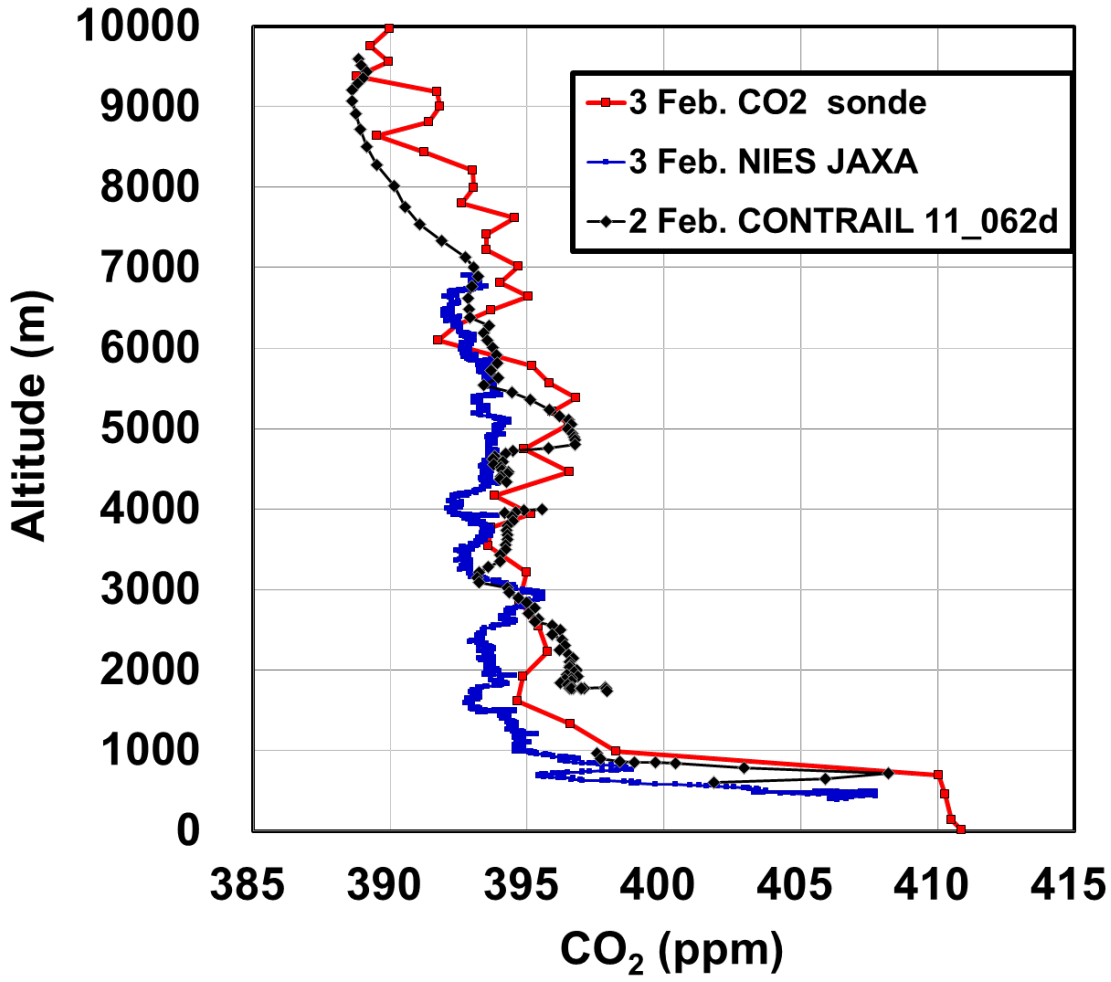

824

825

826 **Figure 8**. The CO_2 vertical profiles obtained by the CO_2 sonde (circles connected with red lines),

827 NIES/JAXA chartered aircraft data (dots connected with purple lines) on February 3rd, and

828 CONTRAIL data (diamonds connected with black lines) on February 2nd, 2011.

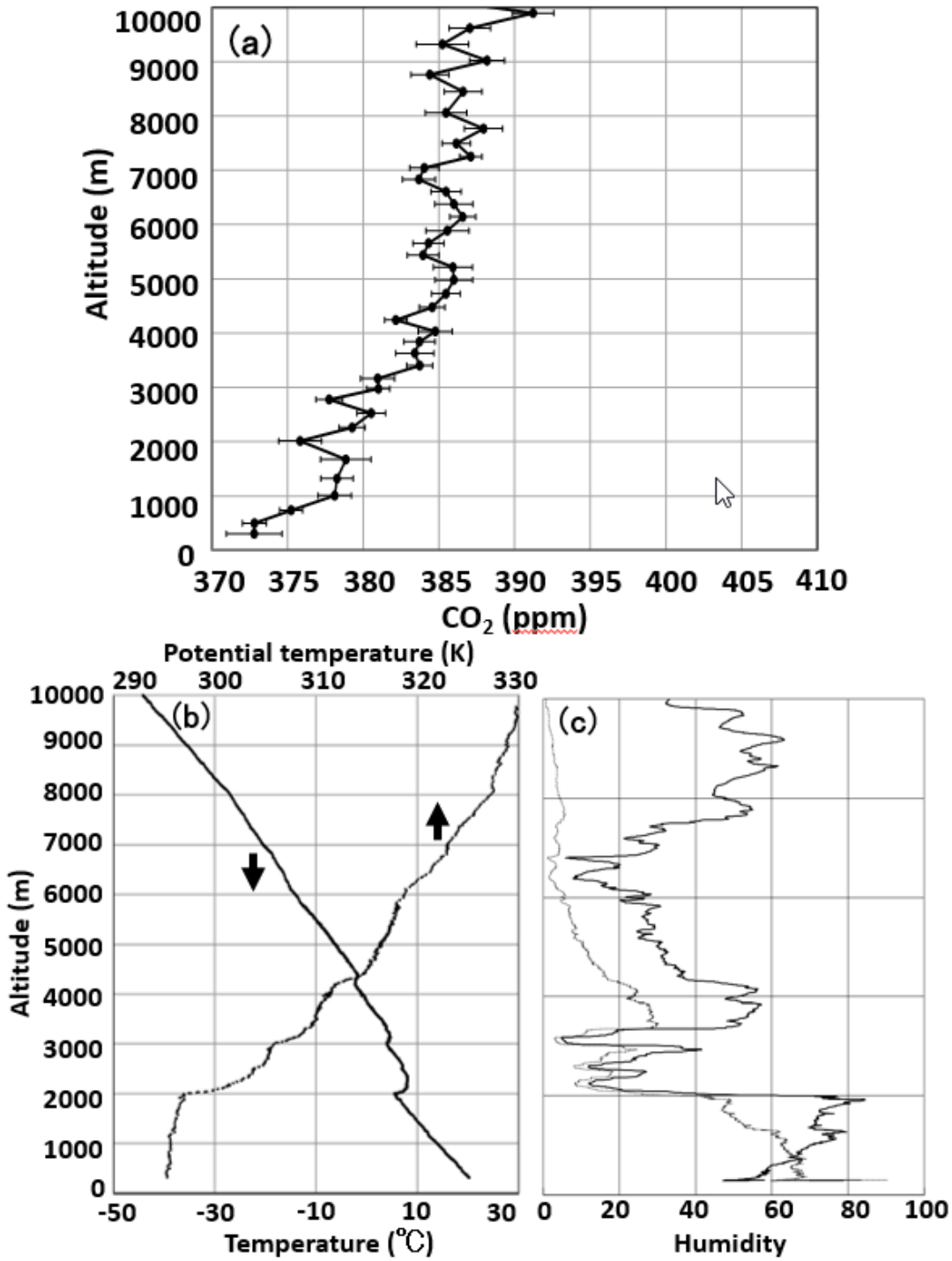

829 **Figure 9**. Profiles of (a) CO_2 mole fraction, (b) temperature (solid line) and potential temperature
830 (dotted line), and (c) relative humidity (Solid line, %) and water mol fraction (dotted line, unit
831 1/5000 mol/mol) observed over a forest area, Moshiri in Hokkaido, Japan by the balloon launched on
832 August 26, 2009 at 13:30 (LST). The black circles with error bars in panel (a) represent the data
833 obtained by the CO_2 sonde.

834

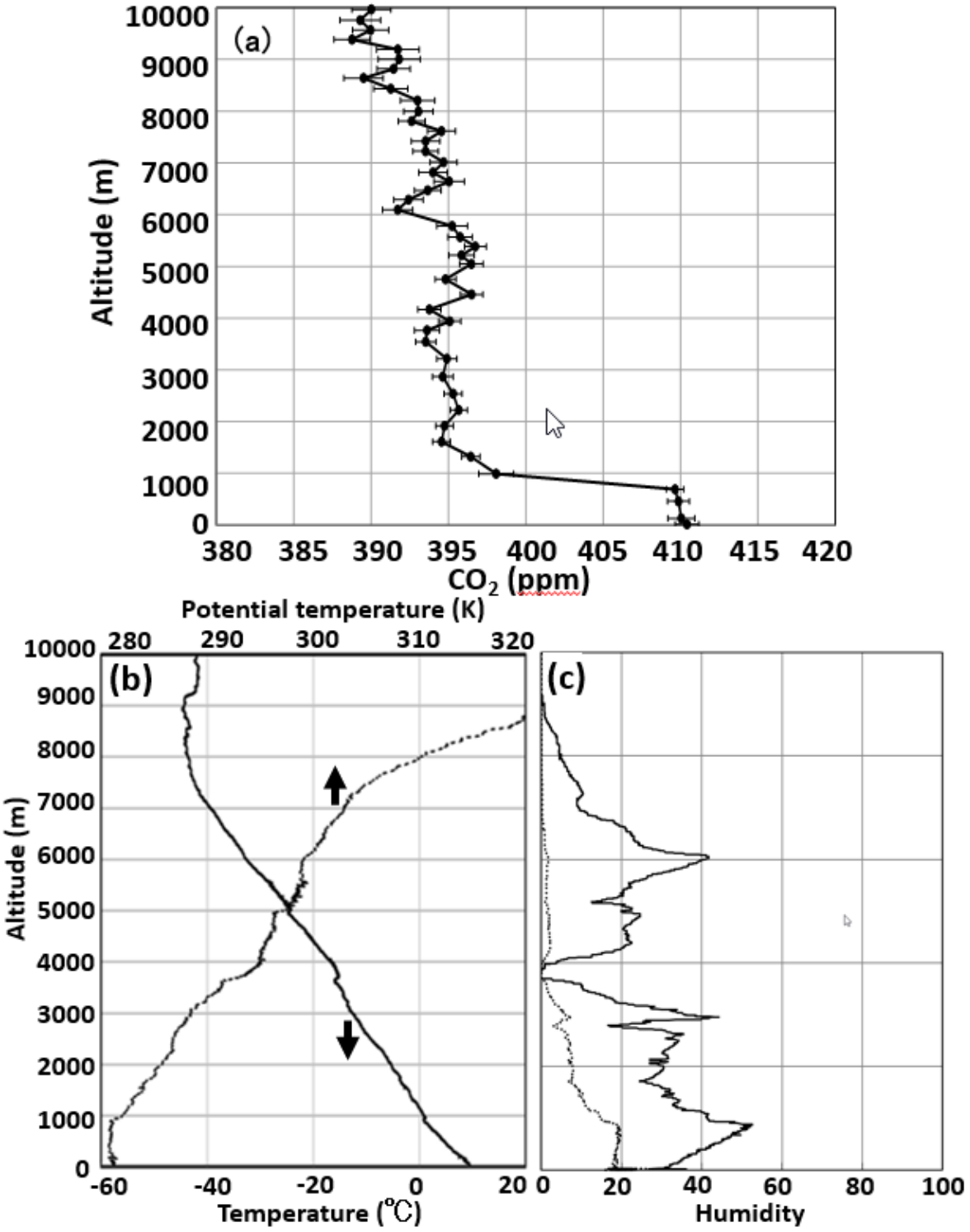

835 **Figure 10**. Profiles of (a) CO_2 mole fraction, (b) temperature (solid line) and potential temperature
836 (dotted line), and (c) relative humidity (Solid line, %) and water mol fraction (dotted line, unit 1/5000
837 mol/mol) observed over an urban area, Moriya near Tokyo on February 3rd, 2011 at 13:10 (LST).
838